

Multi-view Structural Convolution Network for Domain-Invariant Point Cloud Recognition of Autonomous Vehicles

Younggun Kim[Ⓜ], Beomsik Cho[Ⓜ], Seonghoon Ryoo[Ⓜ], and Soomok Lee[†][Ⓜ]

Abstract—Point cloud representation has recently become a research hotspot in the field of computer vision and has been utilized for autonomous vehicles. However, adapting deep learning networks for point cloud data recognition is challenging due to the variability in datasets and sensor technologies. This variability underscores the necessity for adaptive techniques to maintain accuracy under different conditions. In this paper, we present the Multi-View Structural Convolution Network (MSCN) designed for domain-invariant point cloud recognition. MSCN comprises Structural Convolution Layers (SCL) that extract local context geometric features from point clouds and Structural Aggregation Layers (SAL) that extract and aggregate both local and overall context features from point clouds. Additionally, our MSCN enhances feature representation robustness by training with unseen domain point clouds derived from source domain point clouds. This method acquires domain-invariant features and exhibits robust, consistent performance across various point cloud datasets, ensuring compatibility with diverse sensor configurations without the need for parameter adjustments. This highlights MSCN’s potential to significantly improve the reliability and domain invariant features in different environments. Our code is available at <https://github.com/MLMLab/MSCN>.

Index Terms—Point cloud-based Autonomous System, LiDAR Point Cloud Classification, Domain-Invariant Feature Representation, Unseen Domain Generation, Domain Generalization.

I. INTRODUCTION

POINT cloud sensors and data have gained significant attention and are utilized in various fields due to their potential to enhance perception capabilities in advanced systems and robotics through accurate point distance measurements. The point cloud data is generated by Light Detection and Ranging (LiDAR) sensors, which produce high-resolution 3D spatial data and offer accurate measurements of the surrounding environment. These point clouds are crucial for various applications, including autonomous vehicles, robotics, and smart infrastructure systems, where accurate environmental understanding is essential.

Despite considerable advances in 2D image-based object recognition, the transition to 3D object recognition from LiDAR-based point clouds remains a largely underexplored area. This is primarily due to the unstructured and unordered

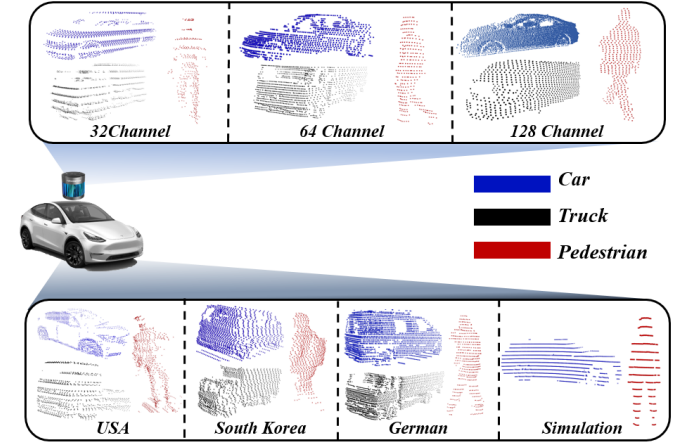


Fig. 1. Illustration of self-driving vehicle recognition scenarios from cross-source point clouds. The properties of the point cloud vary according to the channels in the LiDAR sensor; fewer channels result in sparser point clouds, while more channels create denser point clouds. Additionally, the characteristics of the point cloud differ not only based on the region where the training data was acquired but also between those obtained from simulations and those collected in the real world, which have very different characteristics. Therefore, to maintain consistent recognition capabilities of self-driving cars, robust learning across domains, including changes in LiDAR sensors and areas (real to real and sim to real), is essential.

nature of point clouds, which introduces significant challenges for analysis and interpretation. Unlike 2D images, point clouds lack a clear grid structure, making traditional methods less effective. Overcoming these obstacles is critical for improving the accuracy and reliability of 3D perception systems, which rely heavily on efficient classification techniques.

Moreover, ensuring the robust and consistent trained model is essential for perception, localization and mapping in autonomous vehicles. As depicted in Fig 1, the quality of point clouds obtained through LiDAR sensors heavily depends on the sensor’s resolution. However, LiDAR sensors vary significantly in resolution depending on the manufacturer and its model, leading to substantial differences in the quality of point clouds used for recognition models. Furthermore, real-world objects exhibit significant variation based on its installed location or multi-sensor usage, adding another layer of complexity. These disparities in real-world point clouds have different point cloud patterns and resolutions and result in misjudgments on perception in self-driving vehicles. For example, during the development phase, self-driving vehicles may be trained using high-resolution LiDAR sensors to produce high-quality

Younggun Kim is with Department of Civil Engineering, University of Central Florida, Florida 32816, USA (e-mail: younggun.kim@ucf.edu)

Beomsik Cho and Seonghoon Ryoo are with the Department of Data, Networks and AI, Ajou University, Suwon 16499, Korea. (e-mail: whq-jatlr123@ajou.ac.kr; shryu0512@ajou.ac.kr)

[†]Soomok Lee is the corresponding author and is affiliated with the Department of Mobility Engineering and Department of Artificial Intelligence, Ajou University, Suwon 16499, Korea. (e-mail: soomoklee@ajou.ac.kr)

point clouds. However, in practical deployment scenarios, commercial vehicles may be equipped with low-resolution LiDAR sensors due to cost or other constraints. This disparity can lead to severe performance gaps between the development and deployment environments. Furthermore, when self-driving vehicles are deployed in new unvisited regions or environments during training, models can experience a significant drop in performance[30].

Despite these challenges, recent studies have largely overlooked the domain gap between training and deployment scenarios. While these models may perform well on point clouds with geometric properties similar to the training dataset, their performance often deteriorates in diverse and unseen real-world scenarios. Thus, existing research has failed to address the variability and inconsistencies inherent in real-world point clouds, leaving a critical domain gap in deploying models for various domains in different self-driving platforms.

To process point cloud data from LiDAR, approaches such as point-based [1], [2], [4] and graph-based [3] have been proposed. PointNet [1] processes a point cloud using a neural network to directly consume raw point cloud data, extracting global features through symmetric functions and max pooling to achieve permutation invariance. However, PointNet does not take into account the local structural feature of the point cloud, which may lead to overfit to certain dataset. PointNet++ [2] learns the hierarchical features of point cloud data by stacking multiple learning stages, allowing it to capture detailed local geometric information, but the high computational complexity of this network limits its application to real-world scenarios. PointMLP [4] allows the structural characteristics of point clouds to be extracted using only a simple MLP with residual connections and a geometric affine module without a local geometric extractor, achieving state-of-the-art results towards the ModelNet40 and ScanObjectNN datasets. PointMLP can represent structural features in the overall context of a 3D object, but because it overlooks structural features in the local context, there may be significant performance degradation for outdoor datasets with occlusion or data distribution variance. Dynamic Graph CNN (DGCNN) [3] enhances the understanding of 3D geometric information by using graph-based convolution networks and a k-nearest neighbor strategy to form dynamic graphs, improving local feature comprehension. However, the complexity of DGCNN introduces computational challenges and relies heavily on the precision of input graphs, necessitating innovative solutions for robust feature extraction.

To describe the local information of 3D data more in-depth, some research works [5], [30] utilize deformable 3D kernels that are learnable during the training stage. 3D Graph Convolutional Networks (3D-GCN) [5], distinguished by their incorporation of geometric values and adjustment of network parameters through directional analysis, employ deformable graph kernels to adeptly manage translation, scale, and z-axis rotation. However, this approach cannot properly explain the distances between points in a point cloud, potentially leading to performance degradation in case of domain change. This is mainly because point clouds acquired in the real world have very different spacings between points depending on the dataset. 3D Structural Convolution Network (3D-SCN) [30]

identifies important geometric structures of a point cloud by analyzing the relationship of points between neighborhoods from the standpoint of both distance and direction, enabling domain-invariant point cloud recognition. Nevertheless, because 3D-SCN only trains the local geometric information of a single point cloud, it overlooks the structural information in the overall context and may miss important structural properties of the object.

In this paper, we propose a novel deep learning model named Multi-view Structural Convolution Network (MSCN), which can extract features of 3D point clouds that are robust to domain changes in order to respond to arbitrary domain changes that frequently occur in point cloud recognition scenarios. The MSCN consists of a Structural Convolution Layer (SCL) and a Structural Aggregation Layer (SAL). In the SCL, structural information between points within the point cloud is captured in a local context, while in the SAL, structural information of the point cloud is captured in a global context and embedded into each point across multiple scales. By analyzing the structure of the point cloud from multiple perspectives, our MSCN can achieve highly sophisticated structural feature representation, ensuring stable performance despite domain changes.

In addition, point clouds are inherently irregular and exhibit significant variability depending on the LiDAR resolution and geographic location. To address these real-world irregularities and improve the robustness of the model, we propose a novel approach for generating unseen point clouds based on source point clouds. Inspired by the Progressive Domain Expansion Network [14] proposed for single-domain generalization in 2D images, we extend this concept to 3D point cloud scenarios. By repeatedly generating virtual point clouds of new domains and training the model with these alongside the existing source point clouds, the model learns to generalize effectively to unseen point clouds encountered in real-world scenarios. This process enables the model to achieve greater invariance to domain changes and maintain consistent performance in various real-world conditions.

The main contributions of this study can be summarized in three folds as follows:

- We propose a Multi-view Structural Convolution Network (MSCN) that extracts structural features of point clouds from both specific local and overall contexts, strengthening feature robustness, especially for self-driving datasets including occluded point clouds and differing characteristics between different domains.
- We propose a point cloud domain expansion framework by modifying the 2D Progressive Domain Expansion Network (PDEN)[14] for effectively generating unseen domain point clouds, utilizing these generated virtual point clouds to train the model, thereby enhancing the MSCN’s robustness to domain changes.
- We propose a synthetic point cloud dataset to evaluate the consistent performance of our model when transitioning from simulation to the real world. Furthermore, we demonstrate the data-invariant performance of the proposed MSCN (Multi-view Structural Convolution Network) on this synthetic dataset as well as on various

LiDAR-based real-world point cloud datasets, including the nuScenes dataset (32 channels, United States), the KITTI dataset (64 channels, Germany), and the PanKyo dataset (128 channels, South Korea). These demonstrations highlight the robust adaptability of our model to different sensor configurations and locations.

The subsequent sections of this paper are organized as follows. Section 2 presents a comprehensive literature review of 3D point cloud encoding algorithms, domain adaptation methods, and domain generalization methods. Section 3 illuminates the proposed MSCN architecture. Section 4 shows a framework for progressively generating point clouds of unseen domains from a single domain point cloud and learning a feature extractor with the generated point clouds. In Section 5, the paper presents an evaluation of the proposed network using various point cloud datasets acquired from synthetic datasets, real-world indoor dataset, and real-world self-driving vehicle datasets. Finally, Section 6 concludes the paper.

II. RELATED WORKS

A. 3D point cloud deep learning networks: Encoding perspectives

1) *Multi-view-based methods*: Considering that a collection of 2D views can offer significant information for 3D shape recognition compared to traditional manual feature extraction, several studies [15], [16], [17], [18] have explored recognizing 3D shapes from collections of rendered 2D images. Inspired by these works, Hamdi et al. [19] proposed the Multi-View Transition Network (MVTN). This network includes a differentiable module that predicts the optimal viewpoint for a task-specific multi-view network, aiming to enhance 3D shape recognition by addressing limitations of previous multi-view methods. However, multi-view approaches still struggle to fully exploit the geometric relationships inherent in 3D data and extend their applicability to other 3D tasks, such as segmentation and reconstruction.

2) *Voxel-based methods*: To manage the unstructured nature of point clouds, some studies [20], [21], [22] have used voxel grids or voxelized 3D shapes as model inputs, enabling the application of standard 3D CNNs. Researchers like Riegler et al. [23] and Wang et al. [24] have employed octree structures instead of voxels to improve computational efficiency and reduce memory consumption. Despite their focus on the relationships within 3D data and the grouping of point clouds, voxel-based methods often suffer from low classification efficiency due to the inherent sparsity and incomplete information in point clouds.

3) *Point cloud-based methods*: Recent research has increasingly focused on directly processing point clouds using deep learning techniques to fully utilize the information they contain. Aggregating local features is crucial in this process, as it captures rich information from point clouds. For example, PointNet, proposed by Qi et al. [1], is a pioneering study in this area. PointNet directly takes the point cloud as input, transforms it using the T-Net module, learns each point by sharing the full connection, and finally aggregates the features into global features through a max pooling function. However,

PointNet only captures feature information from individual points and global points, without considering the relational representation of adjacent points. This limitation prevents PointNet from effectively performing domain-invariant feature representation.

B. 3D point cloud deep learning networks: Local aggregation

1) *Point-by-point methods*: Qi et al. [2] later proposed PointNet++ as an extension of PointNet. This method processes point clouds hierarchically, with each layer consisting of a sampling layer, a grouping layer, and a PointNet layer. The sampling layer identifies the centroid of the local neighborhood, the grouping layer constructs a subset of this neighborhood, and the PointNet layer captures the relationships between points within the local area. Despite its hierarchical processing, PointNet++ does not fully utilize the prior relationships between points. Ma et al. [4] observed that detailed local geometric information might not be essential for point cloud analysis, leading them to introduce PointMLP, a pure residual network without a complex local geometry extractor. Instead, it includes a lightweight geometric affine module, significantly improving inference speed. PointMLP achieved state-of-the-art results on both the ModelNet40 dataset [27], which is ideal for CAD-based analysis, and the ScanObjectNN dataset [58], which represents real indoor environments. However, this method may struggle with adaptability and consistent performance on real-world outdoor datasets, which are typically more irregular and sparse, due to its lack of precise local geometric information capture.

2) *Graph-based methods*: Wang et al. [3] proposed the Dynamic Graph CNN (DGCNN) for point cloud learning, introducing the edge convolutional (EdgeConv) network module. This module captures local geometric features of point clouds while maintaining arrangement invariance, underscoring the importance of local geometric features for 3D recognition tasks. However, the network is computationally intensive due to the complexity involved in handling dynamic graph structural modifications. The performance of DGCNN largely depends on the quality of the input graph. Suboptimal or perturbed graphs potentially compromise results, and perfecting graph construction methods is complex. To enhance the graphical relationships of point clouds in convolution, Lin et al. [5] proposed using 3D Graph Convolutional Networks to learn the geometric properties of point clouds. This approach considers geometric values and adjusts network parameters based on directional analysis, incorporating deformable graph kernels to handle translation, scale, and z-axis rotation. However, it does not sufficiently account for distances between point clouds, potentially missing detailed point-by-point interval nuances during parameter training. This limitation is particularly relevant for self-driving datasets, which feature small-scale, consistent patterns despite variations in LiDAR technology or underlying dataset changes. For better adaptation to self-driving datasets, Lee et al. [30] proposed 3D Structural Convolutional Networks, which include 3D convolution kernels to train 3D structural perspectives by combining cosine similarity and Euclidean distance terms. This approach enhances stability and

consistent performance across varying point cloud datasets. However, it only captures the local geometric information of individual point clouds, potentially overlooking the overall structural properties of objects.

C. Domain adaptation and Domain generalization algorithms

1) *Domain adaptation*: Recent studies [6], [7] have demonstrated that deep learning models are prone to significant performance degradation when evaluated on out-of-distribution (OOD) datasets, even with minor variations in the data generation process. These studies underscore the limited generalization capacity of deep learning models, which can severely impact their performance in real-world applications. Domain adaptation (DA) [8], [9], [10] has emerged as a strategy to tackle the OOD data challenge by utilizing a subset of data from the target domain. This approach enables a model trained on a source domain with different distributions to adapt to the target domain. The fundamental concept of DA is that, despite differences between source and target domains, common underlying structures or patterns can be leveraged to enhance model performance in the target domain. However, DA assumes the availability of either labeled or unlabeled data from the target domain for model adaptation, a condition not always met in real-world scenarios. Acquiring labeled data from the target domain can be prohibitively time-consuming, expensive, or impractical due to ethical or legal constraints. Additionally, the target domain’s data distribution may remain unclear, complicating the application of conventional DA methods that rely on understanding this distribution.

2) *Single domain generalization*: To address the challenges associated with domain adaptation (DA), many domain generalization (DG) studies [11], [12], [13], [14] particularly those focusing on single domain generalization, have been proposed. Single domain generalization is a particularly challenging form of model generalization where models are trained on a single domain and tested on unseen domains. A promising approach involves learning cross-domain invariant representations by expanding the coverage of the training domain. These methods typically synthesize additional samples in feature space to broaden the data distribution in the training set. Zhang et al. [11] observed that differences in medical images mainly arise in three aspects: image quality, image appearance, and spatial configuration. They augment these aspects through data augmentation. However, this method requires selecting the appropriate type and magnitude of augmentation based on the target domain, which can be challenging for other tasks. Volpi et al. [12] and Qiao [13] synthesize additional data through adversarial learning to enhance model robustness. Nevertheless, this approach has limitations: the types of augmentation are relatively simple, and using too many adversarial examples during training can degrade classifier performance. To mitigate these issues, Li et al. [14] proposed progressively generating multiple domains and learning a feature extractor using both source and generated data. The model employs contrastive learning to develop domain-invariant representations, effectively clustering each class to facilitate better decision boundaries and improve generalization. While this approach equips

models to perform well in real-world scenarios, particularly on previously unseen domains, it is currently only applicable to domain generalization tasks involving well-structured 2D images.

III. MULTI-VIEW STRUCTURAL CONVOLUTION NETWORK(MSCN)

We focus on describing how to obtain domain-invariant features from the LiDAR point cloud and process it for classification. In the Structural Convolution Layer(SCL) section, we first explain how to extract the local context feature of the point cloud, which is achieved by the proposed structural convolution operation. Then, in the SAL section, we describe the feature extraction method from both local context and overall context of point cloud, making the feature representations more robust. Finally, we illustrate the architecture of point cloud classification.

A. Structural Convolution Layer(SCL)

A 3D point cloud object P consists of N points represented by $P = (p_n | n = 1, 2, \dots, N)$. Each p_n represents a 3D coordinate within the three-dimensional space, thus belonging to the set \mathbb{R}^3 . The structural convolution layer (SCL) captures the local structural and geometric characteristics associated with each point p_n . Figure 2 (b) illustrates the i^{th} structural convolution layer, named $SCL(D_{i-1}, D_i)$. First, $SCL(D_{i-1}, D_i)$ has receptive fields denoted R_n^M to capture the relationships between the point p_n and M neighboring points. Specifically, the receptive field for the point p_n is defined as:

$$R_n^M = \{p_n, p_m | \forall p_m \in \mathcal{N}(p_n, M)\}, \quad (1)$$

where $\mathcal{N}(p_n, M)$ formally represents the M nearest neighbor points of p_n . Each p_n has directional vectors within its receptive fields, defined as $d_{m,n} = p_m - p_n$, which will be used later for selecting the farthest neighbors among points p_m in the receptive field and for performing the structural convolution operation. In i^{th} SCL, all points in a point cloud have D_{i-1} dimension feature vectors $F(p) \in \mathbb{R}^{D_{i-1}}$ and features contained within a receptive field can be expressed as $\{F(p_n), F(p_m) | \forall p_m \in \mathcal{N}(p_n, M)\}$ where $F(p_n), F(p_m) \in \mathbb{R}^{D_{i-1}}$. To perform convolution directly on irregular points within the receptive field, SCL utilizes a Direction-based Kernel (K_{dir}^S) and Distance-based Kernel (K_{dist}^S) defined as follows:

$$K_{dir}^S = \{k_{dir}^1, k_{dir}^2, \dots, k_{dir}^{D_i}\} \quad (2)$$

$$K_{dist}^S = \{k_{dist}^1, k_{dist}^2, \dots, k_{dist}^{D_i}\}, \quad (3)$$

where S denotes the number of branches of the direction-based kernels and distance-based kernels. The branches of the directional kernel $k_{dir}^{D_i}$ are defined as $b_{dir}^1, b_{dir}^2, \dots, b_{dir}^S$. Each branches consists of weight $w(b_{dir}^s) \in \mathbb{D}^i, s = 1, 2, \dots, S$ and a directional vector $b_{dir}^s \in \mathbb{R}^3$ indicating the spatial position of $w(b_{dir}^s)$. To provide directionality to these branches, $k_{dir}^{D_i}$ needs to define the center position, which we

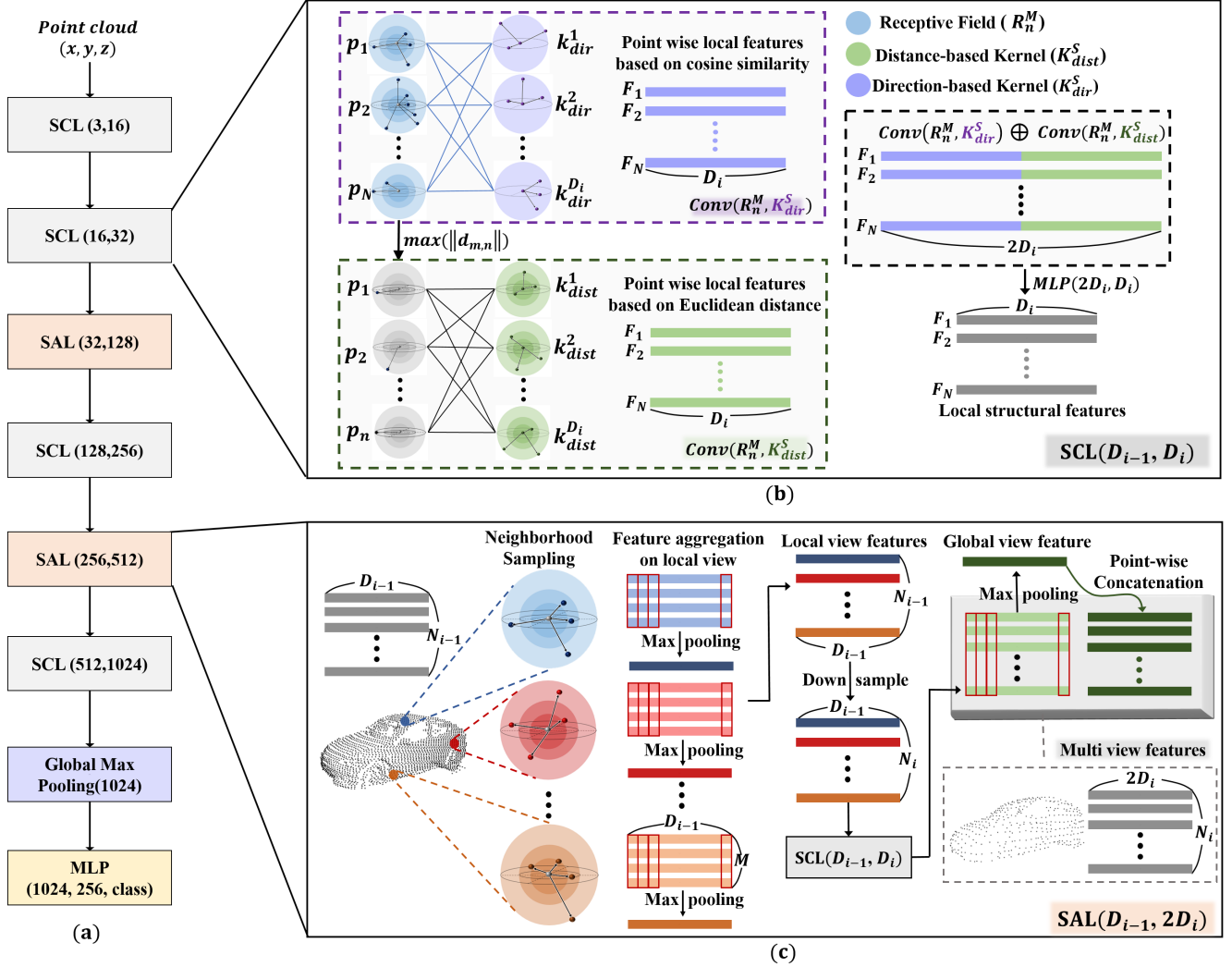


Fig. 2. The Multi-view Structural Convolution Network (MSCN) architecture for 3D point cloud classification comprises several components. (a) The MSCN includes feature extraction layers, specifically Structural Convolution Layers (SCL) and Structural Aggregation Layers (SAL), as well as Global Max Pooling and a multi-layer perceptron (MLP) for classification. (b) SCL is engineered to extract local features from each point. (c) The SAL is designed to combine local context features with overall context features.

set as $b_{dir}^c = (0, 0, 0)$. Since $b_{dir}^s = b_{dir}^s - b_{dir}^c$, learnable parameters in a direction-based kernel can be summarized as $k_{dir}^{D_i} = \{w(b_{dir}^c), (w(b_{dir}^s), b_{dir}^s) | s = 1, 2, \dots, S\}$. On the other hand, the distance-based kernel $k_{dist}^{D_i}$ contains branches defined as $b_{dist}^1, b_{dist}^2, \dots, b_{dist}^S$ and these branches have weights defined as $w(b_{dist}^c)$ and $w(b_{dist}^s)$, indicating weight of the center point and branches respectively. Note that distance-based kernels are designed to analyze point relationships based on Euclidean distance, so the branches of b_{dist} do not have directional vectors. Therefore, trainable parameters in a distance-based kernel can be summarized as $k_{dist}^{D_i} = \{w(b_{dist}^c), w(b_{dist}^s) | s = 1, 2, \dots, S\}$.

Using the defined kernels, we perform convolution on irregular points within a receptive field of a point cloud. Specifically, we first assess the similarity between the features within the receptive field of p_n (i.e. $F(p_n), F(p_m) \forall p_m \in N(p_n, M)$, as specified in Equation 1) and the weight

vectors of the directional kernel K_{dir}^S , centered around b_{dir}^c with S branches (namely, $w(b_{dir}^c), w(b_{dir}^s) \forall s = 1, 2, \dots, S$). We consider every pairing of (p_m, b_{dir}^s) . Consequently, the direction-based convolution between a receptive field and a direction-based kernel can be described as:

$$Conv_{dir}(R_n^M, K_{dir}^S) = \langle F(p_n), w(b_{dir}^c) \rangle + \sum_{s=1}^S \max_{m \in (1, M)} sim(p_m, b_{dir}^s) \quad (4)$$

where the symbol $\langle \cdot \rangle$ denotes the inner product operation, and the function sim calculates the inner product between the features $F(p_m)$ and the directional weights $w(b_{dir}^s)$, utilizing cosine similarity [5] to define this interaction:

$$sim(p_m, b_{dir}^s) = \langle F(p_m), w(b_{dir}^s) \rangle \frac{\langle d_{m,n}, b_{dir}^s \rangle}{\|d_{m,n}\| \|b_{dir}^s\|} \quad (5)$$

The convolution operates between points of all receptive fields and the kernels since k_{dir}^S has directional kernels D_i . Furthermore, to consider the impact of spatial relationships among neighboring points on structural characteristics, the Euclidean distances are calculated from the point p_n to its most distant neighbor and then multiply these distances by the weights of the kernel $k_{dist}^{D_i}$ centered at b_{dist}^c (specifically, $w(b_{dist}^c), w(b_{dist}^s), \forall s = 1, 2, \dots, S, w(b_{dist}^c), w(b_{dist}^s) \in w_{dist}$). We consider all possible combinations of (p_m, b_{dist}^s) to perform the distance-based convolution that merges the receptive fields with the kernels, expressed as:

$$Conv_{dist}(R_n^M, K_{dist}^S) = \sum_{s=1}^S w_{dist} \times \max_{m \in (1, M)} (\|d_{m,n}\|) \quad (6)$$

Finally, by concatenating the outputs from the above convolution operations and passing them through an MLP, the structural convolution operation of the structural convolution layer i^{th} , denoted as $SCL(D_{i-1}, D_i)$, is achieved as follows:

$$SCL(D_{i-1}, D_i) = MLP(Conv_{dir}(R_n^M, K_{dir}^S) \oplus Conv_{dist}(R_n^M, K_{dist}^S)) \quad (7)$$

B. Structural Aggregation Layer (SAL)

SAL (D_{i-1}, D_i) is specially designed to capture the structural information of a point cloud from both local and global perspectives. As shown in Figure 2 (c), SAL (D_{i-1}, D_i) receives a point cloud from the previous layer, where all points have high-dimensional local features D_{i-1} as input. This layer first performs neighborhood sampling to construct the receptive fields and then applies channel-wise max-pooling within these receptive fields to aggregate features $F(p), \forall p \in R_n^M$, resulting in a coarse to fine feature representation at the local level. Next, a subset of P is downsampled using a predetermined sampling rate r . These local view aggregation processes can be formulated as:

$$LocalViewAggregation(P_{in}, F_{in}) = (P_{out}, F_{out}) \quad (8)$$

where $P_{in} \in \mathbb{R}^{N_{i-1} \times 3}, P_{out} \in \mathbb{R}^{N_i \times 3}, F_{in} \in \mathbb{R}^{N_{i-1} \times D_{i-1}}, F_{out} \in \mathbb{R}^{N_i \times D_i}$, and $N_i = \frac{N_{i-1}}{r}$. This local feature aggregation operation allows us to learn multi-scale local context features, which are crucial factors for extracting local geometric information.

The downsampled points P_{out} and the fine features locally F_{out} are used as input of $SCL(D_{i-1}, D_i)$ defined in Equation 7, to extract geometric information at a lower scale. This results in effective geometric features across different scales, exhibiting both scale and shift invariance. The output features of $SCL(D_{i-1}, D_i)$ are summarized into a D_i dimensional vector, called the global view feature, which represents the geometric information of the global context of a point cloud. This global view aggregation process can be formulated as:

$$GlobalViewAggregation(P_{in}, F_{in}) = F_{out} \quad (9)$$

where $P_{in} \in \mathbb{R}^{N_i \times 3}, F_{in} \in \mathbb{R}^{N_i \times D_i}$, and $F_{out} \in \mathbb{R}^{D_i}$. By concatenating the global view feature with each row of

output features from $SCL(D_{i-1}, D_i)$, we can obtain multi-view features $F \in \mathbb{R}^{N_i \times 2D_i}$. This concatenation results in $SAL(D_{i-1}, 2D_i)$, the output of this layer, and serves as the input to the next structural convolution layer.

C. Classification Process

For the purpose of point cloud classification, our framework consists of four structural convolution layers and two structural aggregation layers, as illustrated in Figure 2 (a). As the point cloud data passes through these layers, it becomes more refined and is ultimately summarized into a 1024-dimensional vector using a max-pooling operation. Finally, this vector is fed into a multi-layer perceptron (MLP) for classification across the various classes.

IV. PROGRESSIVE DOMAIN EXPANSION PROCESS

In section 3, we explained how to obtain domain-invariant feature representations of point clouds by capturing geometric relationships between points. In this section, we focus on effectively generating unseen domains of 3d point clouds from specific domain point clouds, enabling MSCN to learn more robust feature representations.

A. Generator composition

To effectively generate unseen domains from a source domain, we adopt PDEN with several modifications. PDEN is originally designed for 2D image generation, which is structured into pixels, so we modify it to work with irregular point clouds. Especially, supplementing random sampling accommodates the sparse nature of point cloud patterns, making it easily adaptable to variations in LiDAR channels.

Our goal is to generate k arbitrary point cloud domains from a source point cloud domain. We define k^{th} domain generator as G_k , which converts the original point cloud x in a source domain S into a synthetic point cloud x'_k in an unseen domain S'_k . The generated point cloud and the unseen domain are formulated as:

$$\begin{aligned} x'_k &= G_k(x, n), n \sim N(0, 1) \\ S'_k &= \{G_k(x_i, y_i) \mid (x_i, y_i) \in S_k\} \end{aligned} \quad (10)$$

where $x' \in \mathbb{R}^3$ has the same semantic information as x , but x' and x belong to different domains. We primarily use an autoencoder with AdaIN [34] as a generator. However, since AdaIN was created for image transfer from a source domain to a specific target domain, we use two fully connected layers L_1 and L_2 along with Gaussian noise N to learn appropriate parameters instead of a specific target domain. By modifying AdaIN to handle irregular point cloud features, our generator can be expressed as:

$$\begin{aligned} G_k(x, n) &= G_D(AdaIN_{3D}(G_E(x), n)), n \sim N(0, 1) \\ AdaIN_{3D}(z, n) &= L_1 \frac{z - \mu(z)}{\sigma(z)} + L_2 \end{aligned} \quad (11)$$

where G_E and G_D denote the encoder and decoder, respectively. Note that $\{G_j, j = 1, 2, \dots, k-1\}$ represents an

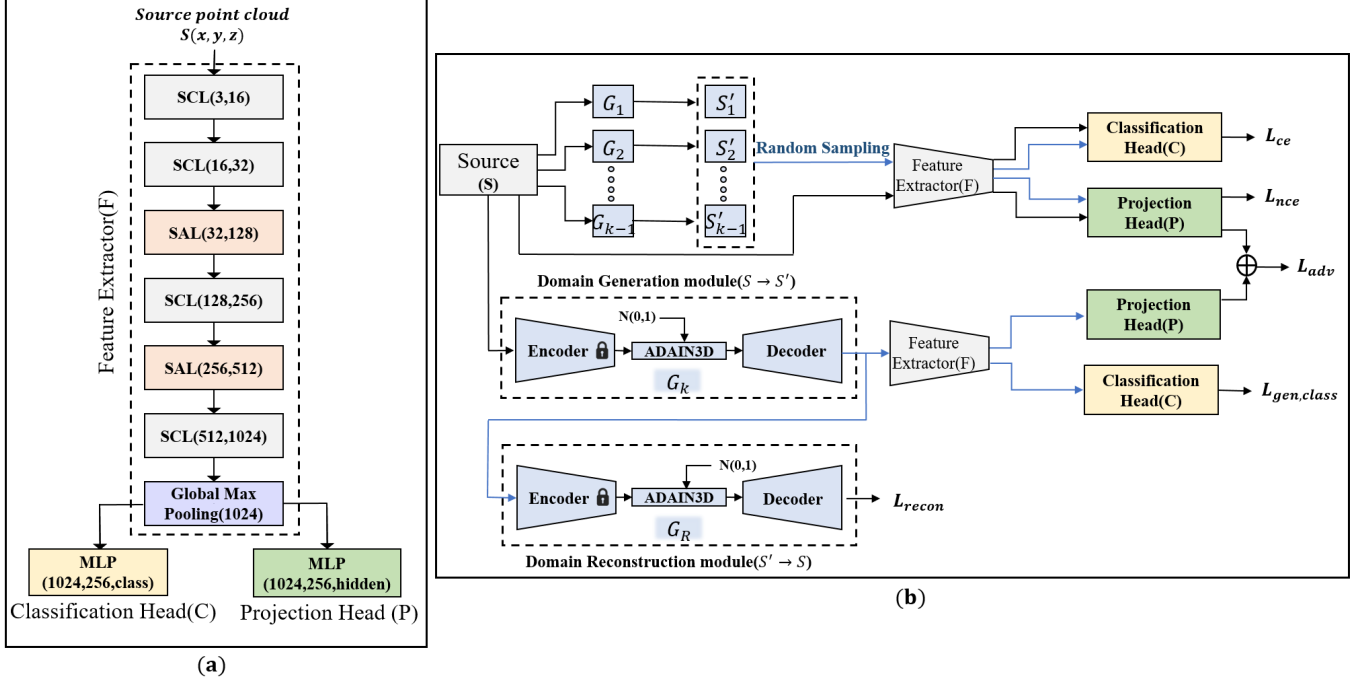


Fig. 3. The architecture for generating unseen domains in MSCN to learn more robust feature representations includes the following components. In (a), the modified MSCN is shown, consisting of a feature extractor (F), a classification head (C), and a projection head (P) with the projection head added for contrastive learning. In (b), the process of generating arbitrary unseen domains and training the MSCN with both source and generated data is illustrated. These generation and training processes are performed alternately.

already trained generator set, which generates the arbitrary unseen domain set $\{S'_j | j = 1, 2, \dots, k-1\}$, with G_k being the target generator to train. These generated domain sets will be used by MSCN to learn more domain-invariant feature representations.

B. MSCN training with $\{S'_i\}_{i=1}^{k-1}$

As depicted in Figure 3 (a), a projection head (P) is added to MSCN for contrastive learning, while the feature extractor (F) and classification head (C) remain the same as Figure 2 (a). In the k^{th} domain expansion environment, MSCN is trained with the updated dataset $S \cup \{S'_i\}_{i=1}^{k-1}$, as shown in Figure 3 (b). Specifically, given a batch $B = \{x_i, y_i\}_{i=1}^{2N}$ where x_i is the source point cloud, $x'_i \in \{S'_i\}_{i=1}^{k-1}$ is the synthetic point cloud randomly sampled from the unseen domain set, and y_i is the class label. MSCN learns domain-invariant feature representations by minimizing cross-entropy loss and InfoNCE loss [35] as follows:

$$L_{ce}(x_i, y_i) = \min_{F,C} - \sum_{m=1}^M y_i^m \log(C(F(x_i^m)))$$

$$L_{nce}(z_i, z_i^+) = \min_{F,C} - \log \frac{\exp(z_i \cdot z_i^+)}{\sum_{j=1, j \neq i}^{2N} \exp(z_i \cdot z_j)}$$
(12)

where M is the number of label, y_i^m is the m^{th} label of y_i , $z_i = P(F(x_i))$, and $z_i^+ = P(F(x'_i))$. Total losses to train MSCN, named L_{src} , can be summarized as follow:

$$L_{src} = L_{ce}(x_i, y_i) + L_{nce}(z_i, z_i^+) \quad (13)$$

C. Unseen Domain S'_k Generation

To effectively and safely generate domains, we compose the unseen domain generation process as shown in Figure 3 (b). The source domain point cloud x is converted to an unseen domain point cloud x'_k in the domain generation module G_k , which is then used as input for both the MSCN and the reconstruction module G_R . The primary goal of the reconstruction module is to reconstruct x'_k to x to ensure the safety of the decoder G_D and $AdaIN_{3D}$ in G_k . This is achieved by minimizing reconstruction loss defined as:

$$L_{recon} = \min_{G_k, G_R} \|x - G_R(G_k(x, n))\|_2 \quad (14)$$

Secondly, MSCN helps G_k generate unseen domains more reliably by ensuring that x'_k is of the same class as x . This is achieved by minimizing the loss of cross-entropy at the head of the class C , formulated as:

$$L_{gen, ce} = \min_{G_k, F, C} L_{ce}(C(F(G_k(x, n))), y), n \sim N(0, 1) \quad (15)$$

On the other hand, to effectively generate unseen domain, we employ adversarial learning. The generator G_k is trained to maximize the InfoNCE loss while MSCN is trained to minimize the loss. Through adversarial training, G_k will generate unseen domains from which MSCN cannot extract domain-shared representations, thereby enhancing MSCN's ability to

extract cross-domain invariant representations. The adversarial loss is defined as:

$$L_{adv} = \min_{G_K} -L_{nce}^*(P(F(x)), P(F(G_k(x, n)))) \\ + \min_{F, P} -L_{nce}(P(F(x)), P(F(G_k(x, n)))) \quad (16)$$

where L_{nce}^* indicates the modified InfoNCE loss for the adversarial loss to converge, and L_{nce}^* is defined as:

$$L_{nce}^*(z_i, z_i^+) = \sum_i^{2N} \left(1 - \log \frac{\exp(z_i \cdot z_i^+)}{\sum_{j=1, j \neq i}^{2N} \exp(z_i \cdot z_j)}\right) \quad (17)$$

Moreover, We use an additional loss function to encourage G_k to generate more diverse samples.

$$L_{div} = \min_{G_K} \|G_k(x, n_1), G_k(x, n_2)\|_2 \quad (18)$$

Finally, we can effectively and safely generate k^{th} unseen domain S'_k by minimizing the total loss, named L_{unseen} , defined as:

$$L_{unseen} = L_{recon} + L_{gen,ce} + L_{adv} + L_{div} \quad (19)$$

V. EVALUATION

To evaluate the domain-invariant capabilities of the proposed MSCN, we conducted comprehensive experiments using both synthetic datasets and real-world datasets collected from self-driving vehicles. The synthetic dataset experiments aim to verify MSCN’s invariance to geometric transformations, including translation and scaling. These tests provide insights into the model’s ability to maintain performance under controlled yet challenging conditions.

In the real-world dataset experiments, we evaluated MSCN’s robustness in scenarios where the LiDAR resolution differs between training and testing environments. This setup simulates practical conditions in autonomous driving, where sensor configurations may vary. Furthermore, we assessed MSCN’s performance under severe domain shifts, combining both dataset-specific variations and additional transformations such as rotation and translation. Even in these harsh conditions, our MSCN consistently demonstrates robust performance, highlighting its effectiveness in domain-adaptive tasks.

A. Datasets & Implementation Detail

1) *Synthetic Datasets*: We conducted experiments using ShapeNetPart [39] and ModelNet40 [27] datasets. For the ShapeNetPart dataset, we evaluated the proposed MSCN on the part segmentation task, while for the ModelNet40 dataset, we performed object classification. Both experiments followed the standard training settings commonly used in previous work. In addition, specific experiments are conducted comparing MSCN with PointMLP [4] and PointTransformer [38] to demonstrate MSCN’s invariance to geometric transformations

such as translation and scaling. For these experiments, we fixed the number of training epochs for all models to 30 and used a consistent point cloud size of 1024 points. These settings ensured a fair comparison across models and highlighted MSCN’s robustness under varying geometric transformations.

2) *Real-world Indoor Dataset*: ScanObjectNN[58] is a challenging dataset of 3D real-world object point clouds, comprising approximately 15,000 instances categorized into 15 classes. It includes three commonly used variants—OBJ BG, OBJ ONLY, and PB T50 RS—that progressively increase in difficulty. The experimental setup adheres to the standard training configurations typically employed in previous studies.

3) *Real-World Self-Driving Vehicle Datasets*: We conducted experiments using three real-world point cloud datasets, namely KITTI[25], PanKyo[30], and nuScenes[26], as well as a synthetic dataset from the MORAI simulator[31]. These datasets, accessible through the following link ¹, originate from various countries and manufacturers, making them crucial for evaluating the inference capacity of the model and the robustness to domain shifts.

Each dataset has a different number of channels. Specifically, nuScenes and the synthetic dataset have 32 channels, KITTI has 64 channels, and PanKyo has 128 channels. These variations help to assess the robustness of the methods. We set the number of classes for the realistic datasets to three, which include car, truck, and pedestrian, while the synthetic datasets have two classes including car and pedestrian.

Comparisons between our methods are conducted, including MSCN and MSCN[†], and previous methods including PointNet[1], PointNeXt[29], PointMLP[4], DGCNN[3], GCN[5], SCN[30], PointTransformer[38], and PointMamba[37]. PointMamba was first pre-trained on ShapeNet[39] and then trained on KITTI, PanKyo, and nuScenes for the classification task. The networks were evaluated through the object classification accuracy and the evaluation metric [32], [33].

To prevent overfitting, which could lead to incorrect classification performance in domain change scenarios, the number of training epochs for all methods, except MSCN[†], is limited to 10. MSCN[†] indicates that applying the unseen domain generation methods to MSCN. For MSCN[†], a new domain is generated every 15 training cycles and this process is repeated 20 times, resulting in a total of 300 epochs.

Furthermore, we use a pre-trained MSCN as the feature extractor in MSCN[†] and pre-trained SCL as the generator encoders in MSCN[†]. This approach ensures the appropriate preservation of features from the source dataset during the generation of unseen domains. The generator encoders are not updated during training.

We set the batch size to 16 and the learning rate to 0.0004 for all methods. The number of branches (S) is set to 1 and the number of neighbors (M) is set to 3 for all graph-based

¹<https://sites.google.com/site/cvsmlee/dataset>

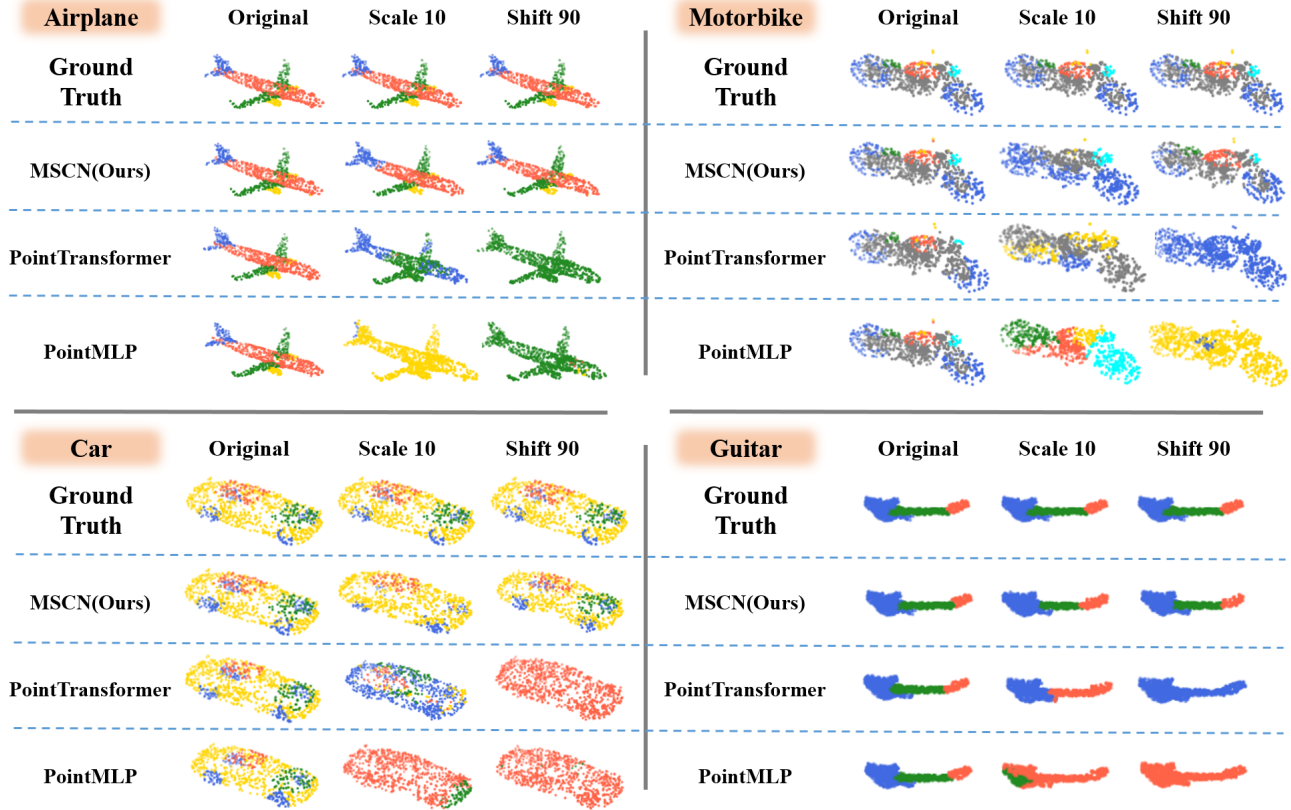


Fig. 4. Examples of geometric transformation on ShapeNetPart[21], where **scale 10** represents a transformation where the original point cloud is scaled by a factor of 10, while **shift 90** indicates a random translation of the point cloud by a distance of 90 units.

Method	#points	mIOU (%)
PointCNN [41]	2048	86.1
PointNet++ [2]	2048	85.1
SO-Net [42]	1024	84.6
SpiderCNN [48]	2048	85.3
PointConv [44]	2048	85.7
KPCConv [43]	2048	86.4
CRFConv [52]	2048	85.5
DensePoint [45]	2048	86.4
RS-CNN w/o vot. [46]	2048	85.8
RS-CNN w/ vot. [46]	2048	86.2
PointASNL [47]	2048	86.1
PointNet [1]	2048	83.7
DGCNN [3]	2048	85.1
PointMamba [37]	2048	86.2
PointMLP [4]	2048	86.1
PointTransformer[38]	2048	86.6
MSCN(Ours)	1024	84.8

TABLE I
OBJECT PART SEGMENTATION RESULTS ON SHAPENETPART[21],
GROUPED BY DATASET. MIOU VALUES ARE REPORTED FOR EACH
METHOD AND DATASET.

methods within receptive fields, including GCN, SCN, MSCN, and MSCN[†]. Both DGCNN and point-by-point methods such as PointNet, PointNeXt, and PointMLP require point cloud normalization, so we conducted point cloud normalization for these methods. All experiments were carried out on a workstation with a deca-core Intel Xeon Silver 4210R CPU clocked at 2.4 GHz and an NVIDIA RTX A5000 GPU with 24GB of memory.

B. Evaluation on Synthetic Datasets: Robustness to geometric deformation

We first conducted experiments on the ShapeNetPart [21] dataset for part segmentation. Table 4 summarizes the part segmentation results, where mIoU values are reported for each method. Our MSCN achieves performance comparable to state-of-the-art (SOTA) models, despite using only 1024 points, unlike other SOTA models that rely on 2048 points. While SOTA models exhibit high performance on the given dataset, MSCN’s performance is slightly inferior compared to SOTA models. This performance gap can be explained by the inherent trade-off between robustness and accuracy, as discussed in [59]. Our MSCN were designed to generalize well to harsh or out-of-distribution scenarios while preserving accuracy on natural data. However, Zhang et.al[59] showed this approach often leads to a shift in focus from minimizing standard classification errors (natural error) to improving robustness, which can degrade accuracy in ideal.

To further evaluate robustness of MSCN, we conducted experiments to visualize the robustness of MSCN compared to PointMLP and PointTransformer under geometric transformations. Figure 4 illustrates the results of scaling and translating point clouds. MSCN demonstrates robust part segmentation even under significant geometrical transformations, whereas PointMLP and PointTransformer show sensitivity to these changes, resulting in suboptimal

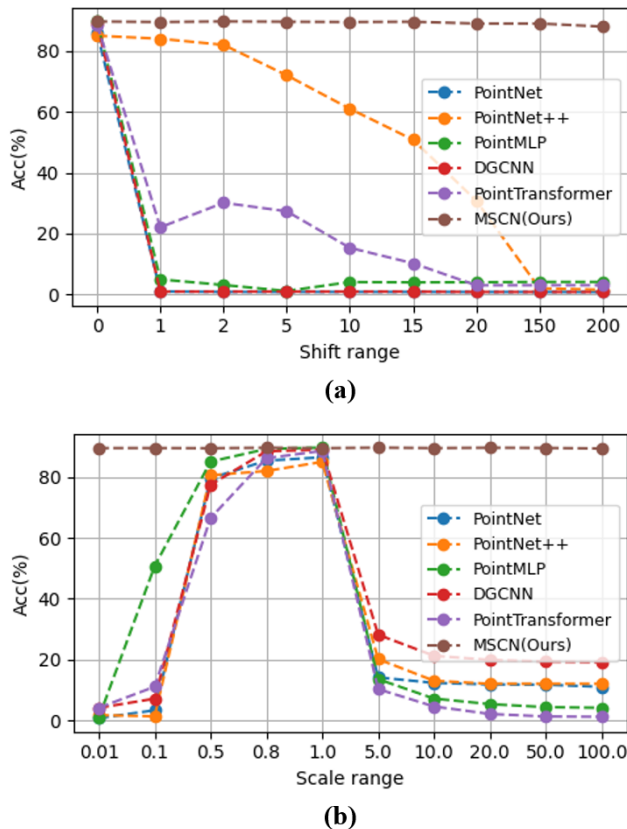


Fig. 5. Evaluation of Geometrical Invariance Properties on ModelNet40[27]. Each graph illustrates the accuracy of various models under specific geometric transformations applied to point clouds. (a) Translation: Accuracy as the translation magnitude increases sequentially from 0 to 200 units. (b) Scaling: Accuracy as the scale factor increases sequentially from 0.01 to 100.

Method	# points	Acc. (%)
PointNet++ [2]	1024	93.8
MVTN [19]	1024	93.8
RepSurf-U [51]	1024	94.4
PointTransformer V2 [49]	1024	94.2
GPSFormer [50]	1024	94.2
PointNet [1]	1024	89.2
PointNeXt [29]	1024	94.0
DGCNN [3]	1024	92.9
GCN [5]	1024	92.1
PointMamba [37]	1024	93.6
PointMLP [4]	1024	94.5
PointTransformer [38]	1024	93.7
MSCN(Ours)	1024	92.2

TABLE II
CLASSIFICATION RESULTS ON MODELNET40 [27].

performance. These results emphasize MSCN’s ability to generalize effectively across various geometric variations.

Furthermore, we conducted experiments on the ModelNet40 [27] dataset for object classification. Table 5 presents the classification results, where MSCN is slightly lower than some state-of-the-art (SOTA) models. Although SOTA models demonstrate strong performance on this dataset, their sensitivity to geometric transformations can result in significant performance degradation in more challenging scenarios. To further investigate this, Figure 5 illustrates

the performance of models under geometric transformations such as translation and scaling. MSCN consistently exhibits robust performance across all transformations, maintaining stable accuracy despite severe geometric changes. In contrast, other methods experience substantial drops in accuracy, highlighting their vulnerability to such transformations. These results underscore the strength of MSCN in terms of geometrical invariance, demonstrating its potential for real-world applications where robustness to geometric variations is critical.

However, it is important to note that ModelNet40 and ShapeNetPart are derived from CAD models, which are generated in highly idealized environments. In contrast, real-world point clouds are often sparse and only capture surface-level details, which makes them fundamentally different from synthetic datasets. To address this disparity, we extended our experiments to real-world point clouds, enabling a more comprehensive evaluation of our MSCN’s performance in practical scenarios.

C. Evaluation on Indoor Real-World Datasets: Comparable Performance and Robustness

We conducted experiments on the ScanObjectNN [58] dataset to evaluate the performance of MSCN on real-world indoor point clouds. Table III summarizes the classification results, demonstrating that MSCN achieves performance comparable to the state-of-the-art (SOTA) models in standard evaluation settings. Furthermore, MSCN exhibits remarkable robustness under geometric transformations such as scaling and translation, maintaining stable performance and demonstrating its strength in handling these variations.

However, it is important to note that ScanObjectNN consists of point clouds captured in indoor environments, which are relatively dense and structured. In contrast, point clouds captured in outdoor environments, such as those used in autonomous driving, are significantly sparser and often acquired under harsh conditions, including occlusions and uneven sampling. To address these challenges, we extended our experiments to self-driving vehicle datasets, enabling a more comprehensive evaluation of MSCN’s robustness in real-world scenarios.

D. Evaluation on Self-Driving Datasets: Cross-Domain Robustness

Our methods focus on maintaining consistent object recognition performance regardless of the type of point cloud data encountered. This means they are designed to work well not only with the data they were originally trained on but also with data from different sources. To thoroughly assess their effectiveness, we conducted two types of evaluations. Both intra-domain and cross-domain performances were evaluated to provide a comprehensive understanding of the capabilities of the methods and to ensure their reliability and effectiveness across various datasets.

Method	PT	RT	RS	OBJ_BG \uparrow	OBJ_ONLY \uparrow	PB_T50_RS \uparrow
<i>With Self-supervised Pre-training</i>						
Transformer [38]	OcCo [55]	\times	\times	84.85	85.54	78.79
Point-BERT[54]	IDPT [56]	\times	\times	88.90	88.10	85.01
MaskPoint[53]	MaskPoint[53]	\times	\times	89.10	88.20	85.02
PointMamba [37]	IDPT [56]	\times	\times	89.10	88.10	85.03
<i>Supervised Learning Only</i>						
PointNet [1]	\times	\times	\times	73.3	79.2	68.0
PointNet++ [2]	\times	\times	\times	82.3	84.3	75.4
DGCNN [3]	\times	\times	\times	82.6	86.2	78.1
PointCNN [41]	\times	\times	\times	86.1	85.5	80.5
PointNeXt [29]	\times	\times	\times	-	-	87.7 \pm0.4
PCT[57]	\times	\times	\times	-	-	82.48
PointMamba [37]	\times	\times	\times	88.30	87.78	82.48
PointMLP [4]	\times	\times	\times	-	-	85.4 \pm 0.3
PointTransformer [38]	\times	\times	\times	79.86	80.55	77.24
MSCN(Ours)	\times	\times	\times	89.33	86.91	83.03
<i>Translation and Scale Invariance of MSCN</i>						
MSCN(Ours)	\times	\checkmark	\times	89.67	86.30	83.83
MSCN(Ours)	\times	\times	\checkmark	89.67	86.30	83.83
MSCN(Ours)	\times	\checkmark	\checkmark	89.66	86.30	83.83

TABLE III

CLASSIFICATION RESULTS ON THE SCANOBJECTNN[58] DATASET. THIS TABLE SUMMARIZES THE PERFORMANCE OF VARIOUS METHODS UNDER DIFFERENT EXPERIMENTAL SETTINGS, INCLUDING SELF-SUPERVISED PRETRAINING, SUPERVISED LEARNING, AND THE EVALUATION OF MSCN’S TRANSLATION AND SCALE INVARIANCE. PT INDICATES PRETRAINED MODELS, RT REPRESENTS RANDOM TRANSLATION, AND RS DENOTES RANDOM SCALING.

Train/Test Dataset	Method	Acc.(%)
KITTI (German, 64CH)	PointNet [1]	99.5
	PointNeXt [29]	99.6
	PointMLP [4]	99.9
	DGCNN [3]	99.6
	GCN [5]	96.3
	SCN [30]	99.2
	PointTransformer [38]	99.3
	PointMamba [37]	100
	MSCN(ours)	97.5
Pankyo (Korea, 128CH)	PointNet [1]	92.6
	PointNeXt [29]	93.6
	PointMLP [4]	96.6
	DGCNN [3]	95.5
	GCN [5]	93.4
	SCN [30]	93
	PointTransformer [38]	98.5
	PointMamba [37]	95.5
	MSCN(ours)	94.5
nuScenes (US, 32CH)	PointNet [1]	95.6
	PointNeXt [29]	95.5
	PointMLP [4]	94.7
	DGCNN [3]	95.5
	GCN [5]	87.6
	SCN [30]	90.8
	PointTransformer [38]	96.2
	PointMamba [37]	97.9
	MSCN(ours)	92

TABLE IV

INTRA-DOMAIN CLASSIFICATION RESULTS ON KITTI [25], nuSCENES [26], AND PANKYO [30] DATASETS. THE BOLD BLACK, BLUE INDICATE THE FIRST AND THE SECOND BEST PERFORMANCE ON EACH SCENARIO, RESPECTIVELY.

First, the performances are demonstrated within the KITTI[25], nuScenes[26], and PanKyo[30] datasets to capture classification performance seamlessly using the training dataset on the test dataset. Table IV shows the

classification performance within a single domain. These results measure the model’s ability to classify point clouds within the same domain used for training. While MSCN achieves competitive results, it lags slightly behind the SOTA methods in terms of accuracy. For example, the average intra-domain accuracy of MSCN across all datasets is 94.7%, compared to PointTransformer’s 98%. This performance gap can be explained from the bias-variance trade-off [40]. MSCN, designed for robust domain-invariant feature extraction, prioritizes reducing model variance to generalize effectively across diverse domains. As a result, its intra-domain performance exhibits slightly higher bias, which is a common trade-off observed in models designed with high generalization capacity. Specifically, while other SOTA models may minimize bias within the training domain, they often exhibit poor performance in domain-shift scenarios due to higher variance.

To demonstrate MSCN’s robustness, we further evaluated its performance under cross-domain scenarios as illustrated in Table V, where substantial domain shifts between training and testing datasets. PointNet, PointNeXt, PointMLP, DGCNN, PointTransformer, and PointMamba demonstrate good performance when the domain shifts from simulation to the real world (Sim2Real) but show significantly lower performance when shifting from one real-world dataset to another (Real2Real). On the other hand, GCN and SCN show robust performance in Real2Real domain change scenarios but are sensitive in Sim2Real scenarios.

However, our MSCN demonstrates robust performance in both Real2Real and Sim2Real scenarios compared to the aforementioned methods. In particular, MSCN surpasses all SOTA methods with an average cross-domain accuracy of

Methods	Param. (M)	KITTI (64CH)		PanKyo (128CH)		nuScenes (32CH)		Simulation (32CH)			Average Acc(%)
		PanKyo	nuScenes	KITTI	nuScenes	KITTI	PanKyo	KITTI	PanKyo	nuScenes	
PointNet [1]	3.0	59.3	62.8	6.2	21.8	36.3	47.9	82.6	78.5	71.8	51.9
PointNeXt [29]	14.1	67.6	31.4	5.8	17.3	31.6	18.6	82.7	88.6	76.1	46.6
PointMLP [4]	13.2	17.7	80.4	87.7	64	47.1	15.2	81	84.6	35.2	57
DGCNN [3]	4.2	14.5	38	6.2	25.6	72.2	20.1	81.2	82.7	94.6	48.3
GCN [5]	1.2	60.9	60.6	83	64.1	92.8	86.2	20.7	16.7	23.8	56.5
SCN [30]	3.5	42.6	72.3	84.4	67.3	92.1	74.3	30.9	48.4	29.1	60.2
PointTransformer [38]	9.6	7.9	88.1	77.3	73.3	79.1	8.8	80.5	87.1	94.0	66.2
PointMamba[37]	12.3	6.6	90.1	11.5	37.5	61.6	30.6	96.9	90.9	89.3	57.2
MSCN(ours)	4.2	81.7	75.3	88.2	78.5	92.8	84.8	83.5	83.9	69.2	82

TABLE V

CROSS-DOMAIN CLASSIFICATION RESULTS ON KITTI [25], NUSCENES [26], PANKYO [30], AND SIMULATION [31] DATASETS. THE BOLD BLACK, BLUE INDICATE THE FIRST AND THE SECOND BEST PERFORMANCE ON EACH SCENARIO, RESPECTIVELY.

Methods	Param.(M)	KITTI			PanKyo			nuScenes			Simulation			Average Time(ms)
		KITTI	PanKyo	nuScenes	KITTI	PanKyo	nuScenes	KITTI	PanKyo	nuScenes	KITTI	PanKyo	nuScenes	
PointNet [1]	3.0	4.1	2.0	0.8	3.9	1.9	0.7	3.9	2.2	0.8	4.0	2.1	0.8	2.3
PointNeXt [29]	14.1	38.2	37.5	37.3	38.2	37.4	37.1	38.1	37.5	37.2	38.1	37.4	37.2	37.6
PointMLP [4]	13.2	32.4	31.1	31.0	32.4	31.1	31.0	32.6	31.4	31.1	32.5	31.2	31.1	31.6
DGCNN [3]	4.2	10	8.8	8.2	10	8.8	8.2	10	8.8	8.1	10.1	8.9	8.2	9.0
GCN [5]	1.2	3.6	2.9	2.6	3.6	3.0	2.6	3.6	2.9	2.6	3.6	2.8	2.5	3.0
SCN [30]	3.5	4.0	3.2	2.8	4.2	3.4	2.8	4.5	3.3	2.9	4.1	3.1	2.7	3.4
PointTransformer [38]	9.6	36.5	34.6	34.1	35.8	36.3	35.3	36.5	34.6	34.1	36.4	34.5	34.0	35.2
PointMamba[37]	12.3	5.4	4.1	3.4	5.4	4.1	3.4	5.5	4.1	3.4	5.4	4.1	3.4	4.3
MSCN(ours)	4.2	4.7	3.6	3.1	4.9	3.6	3.2	4.4	3.6	3.2	4.7	3.6	3.1	3.8

TABLE VI

INFERENCE TIME PER POINT CLOUD ON KITTI [25], NUSCENES [26], PANKYO [30], AND SIMULATION [31] DATASETS. ALL VALUES ARE MEASURED IN MILLISECONDS (MS).

Traning Dataset	Test Dataset	Layer Configuration	Acc.(%)
KITTI	PanKyo	only SCL MSCN(SCL+SAL)	78.9 81.7
	nuScenes	only SCL MSCN(SCL+SAL)	74.8 75.3
PanKyo	KITTI	only SCL MSCN(SCL+SAL)	84.9 88.2
	nuScenes	only SCL MSCN(SCL+SAL)	71.6 78.5
nuScenes	KITTI	only SCL MSCN(SCL+SAL)	92.1 92.8
	PanKyo	only SCL MSCN(SCL+SAL)	78.4 84.8
Simulation	KITTI	only SCL MSCN(SCL+SAL)	71.3 83.5
	PanKyo	only SCL MSCN(SCL+SAL)	75.1 83.9
	nuScenes	only SCL MSCN(SCL+SAL)	45.9 69.2

TABLE VII

LAYER CONFIGURATION EVALUATION RESULTS ON KITTI [25], NUSCENES [26], PANKYO [30], AND SIMULATION [31] DATASETS. THE BOLD BLACK INDICATES THE BEST PERFORMANCE ON EACH SCENARIO.

82%, significantly higher than PointTransformer’s 66.2%. This 15.8% improvement highlights the effectiveness of MSCN in handling domain shifts, which is critical for real-world applications such as autonomous driving and robotics.

The results collectively demonstrate that while MSCN’s intra-domain performance is slightly lower due to the bias-variance trade-off, its superior generalization ability in cross-domain scenarios validates its design focus on robust domain-invariant feature extraction.

Furthermore, Table VI presents the inference time required to predict the class of a single point cloud in both intra-

Traning Dataset	Test Dataset	Method	Acc.(%)	Time (ms)
KITTI	KITTI	MSCN	97.5	4.7
		MSCN [†]	99.7	4.4
	PanKyo	MSCN	81.7	3.6
PanKyo	KITTI	MSCN	75.3	3.1
		MSCN [†]	82.7	3.1
	nuScenes	MSCN	88.2	4.9
PanKyo	PanKyo	MSCN	94.5	3.6
		MSCN [†]	98.3	3.5
	nuScenes	MSCN	78.5	3.2
nuScenes	KITTI	MSCN	92.8	4.4
		MSCN [†]	95.4	4.2
	PanKyo	MSCN	84.8	3.6
Simulation	PanKyo	MSCN	86.6	3.6
		MSCN [†]	92	3.2
	nuScenes	MSCN	94.6	3.0
Simulation	KITTI	MSCN	83.5	4.7
		MSCN [†]	95.7	4.4
	PanKyo	MSCN	83.9	3.6
nuScenes	MSCN [†]	96.2	3.5	
		MSCN	69.2	3.1
		MSCN [†]	87.1	3.1

TABLE VIII

UNSEEN DOMAIN GENERATION EFFECTS ON KITTI [25], NUSCENES [26], PANKYO [30], AND SIMULATION [31] DATASETS. THE BEST RESULTS ARE GIVEN IN BOLDFACE. THE † MARK INDICATES THE METHOD TRAINED WITH OUR UNSEEN DOMAIN GENERATION METHOD, ACHIEVED FROM EQUATION 13 AND EQUATION 19.

domain and cross-domain settings. Models such as PointMLP, PointNeXt, and PointTransformer exhibit higher inference times due to their significantly large number of parameters. In contrast, although PointMamba is also Transformer-based and has a large parameter count, its inference time is relatively low. This efficiency can be attributed to its design, which likely

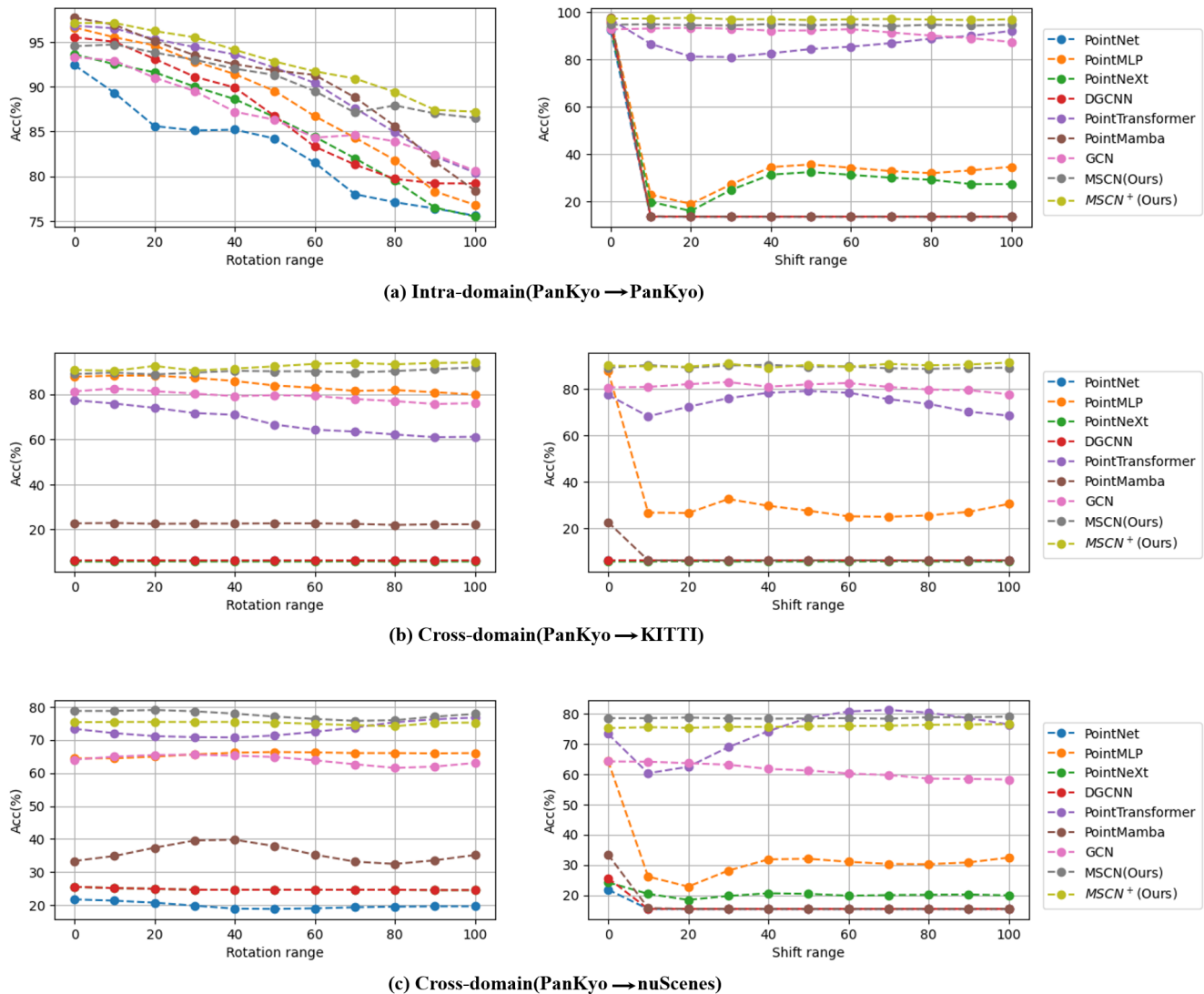


Fig. 6. Evaluation of Invariance Properties. All models were trained on the PanKyo [30] dataset and then tested on (a) PanKyo[30], (b) KITTI[25], and (c) nuScenes[26] datasets. The graphs on the left illustrate the performance of the models when point clouds were rotated along the upward direction. The graphs on the right show the results when the models were tested with randomly shifted point clouds within a certain distance in all directions. For example, the right graph in (a) presents the results of 11 experiments (from 0 to 100 shift) conducted in an Intra-domain setting. Each experiment measures the performance of the models when the point clouds are randomly shifted within a specified maximum distance range.

focuses on reducing FLOPs (Floating Point Operations Per Second) to enhance computational efficiency.

In particular, the average inference time of MSCN is only 3.8 ms, which is well suited for real-world applications such as autonomous driving. Modern rotary LiDAR sensors typically operate at speeds of 10 Hz to 20 Hz, meaning one full rotation takes 0.05 to 0.1 seconds. Given that MSCN can process a single point cloud within 3.8 ms, it is capable of handling multiple scans within a single rotation, ensuring real-time performance without bottlenecking the data pipeline. This efficient processing time, combined with robust cross-domain performance, demonstrates the viability of MSCN for deployment in real-world autonomous systems.

E. Ablation study

In this section, we evaluate the compatibility of layer configurations of MSCN and the performance enhancement when MSCN was trained with synthetic point cloud datasets from our unseen domain generation method. In addition, the invariance properties of MSCN and MSCN[†] are evaluated by conducting experiments on point cloud rotation and shift, further analyzing its robustness across varying domains.

Firstly, to assess the compatibility of layer configurations of MSCN, we compare the cases where there are configurations of both SCL and SAL, and only SCL. The former consists of four SCL and two SAL, which is illustrated in Figure 2 (a). The latter is composed of five SCL that are SCL(3, 32), SCL(32, 64), SCL(64, 128), SCL(128, 256), and SCL(256,

1024). Table VII shows the performance of the methods in layer configurations where domain shift scenarios. MSCN outperforms the case that has only SCL without SAL during all domain shift scenarios, with an average performance that is 7.2% higher than the case that only consist of SCL.

To evaluate the impact of our unseen domain generalization methods on improving the leaning of domain-invariant feature representation, we performed various experiments based on both intra-domain and cross-domain classification, which are illustrated in Table VIII. MSCN[†], which can increase the amount of training without overfitting, performs better than MSCN for single-domain classification. Note that MSCN does not include a domain generation module. With the domain generation module, MSCN[†] demonstrates even more robust performance than MSCN in various domain change scenarios, with an average improvement of 5.8%, indicating that our proposed unseen domain generation method ensures domain generalization ability.

Finally, we compare the robustness of our model in domain shift scenarios, as well as its invariance properties when point clouds undergo rotations and shifts, against other models. To evaluate this, we progressively rotated the point clouds from 0° (no rotation) to 100° in 10° increments and randomly shifted the point clouds from 0 to 100 units.

Figure 4 illustrates six different scenarios where point clouds were subjected to both shifts and rotations in intra-domain and cross-domain settings. In the intra-domain experiments, as the point clouds were gradually rotated, most of the methods showed a sharp decrease in performance, while our MSCN and MSCN[†] exhibited a more gradual decrease, demonstrating their resilience. Furthermore, when point clouds were shifted within the intra-domain setting, our MSCN and MSCN[†] again proved to be the most robust.

Furthermore, in domain shift scenarios, including PanKyo to KITTI and PanKyo to nuScenes, our models outperformed others, maintaining strong performance even as the point clouds were rotated and shifted. This shows that MSCN and MSCN[†] are not only effective in maintaining accuracy, but are also robust to significant geometric transformations in challenging cross-domain environments.

VI. CONCLUSION

In this paper, we introduced MSCN, which learns domain-invariant feature representations by capturing the geometric information of 3D point clouds from the standpoint of both local context and overall context. Moreover, we developed the MSCN through our unseen domain expansion framework, enabling the MSCN to learn more robust feature representations. Our MSCN and MSCN[†] demonstrated the highest performance in cross-domain classification tasks in self-driving data sets, which are derived not only from real-world data, different regions, and sensors, but also from simulators. These results indicate that our method addresses sensor-dependent problems in point cloud classification tasks within the self-driving vehicle field. In light of these findings, our future research endeavors will focus on expanding our method to

object detection tasks for real-world applications that require domain-invariant recognition, such as autonomous driving, robotics, and virtual reality.

ACKNOWLEDGMENT

This work was supported by the Korea National Police Agency(KNPA) under the project 'Development of the autonomous driving patrol service for active prevention and response to traffic accidents' (RS-2024-00403630) and the BK21 FOUR program of the National Research Foundation Korea funded by the Ministry of Education(NRF5199991014091).

REFERENCES

- [1] Charles Ruizhongtai Qi, Hao Su, Kaichun Mo, and Leonidas J. Guibas. Pointnet: Deep learning on point sets for 3d classification and segmentation. In Proceedings of the IEEE conference on computer vision and pattern recognition (CVPR), 2017.
- [2] Charles Ruizhongtai Qi, Li Yi, Hao Su, and Leonidas J. Guibas. PointNet++: Deep Hierarchical Feature Learning on Point Sets in a Metric Space. In Advances in Neural Information Processing Systems (NIPS), pages 5099-5108, 2017.
- [3] Yue Wang, Yongbin Sun, Ziwei Liu, Michael M Bronstein Sanjay E Sarma, and Justin M Solomon. Dynamic Graph CNN for Learning on Point Clouds. *ACM Transactions On Graphics (TOG)*, 38(5):1–12, 2019.
- [4] Xu Ma, Can Qin, Haoxuan You, Haoxi Ran, and Yun Fu. Rethinking Network Design and Local Geometry in Point Cloud: A Simple Residual MLP Framework. In Proceedings of International Conference on Learning Representations (ICLR), 2022.
- [5] Zhi-Hao Lin, Sheng-Yu Huang, and Yu-Chiang Frank Wang. Learning of 3D Graph Convolution Networks for Point Cloud Analysis. *IEEE Transactions on Pattern Analysis and Machine Intelligence*, 44(8):4212–4224, 2021.
- [6] Benjamin Recht, Rebecca Roelofs, Ludwig Schmidt, and Vaishal Shankar. Do Imagenet Classifiers Generalize to Imagenet?. In Proceedings of Machine Learning Research (PMLR), pages 5389–5400, 2019.
- [7] Jingkang Yang, Kaiyang Zhou, Yixuan Li, and Ziwei Liu. Generalized Out-of-Distribution Detection: A Survey. arXiv preprint arXiv:2110.11334, 2021.
- [8] Ziwei Liu, Zhongqi Miao, Xingang Pan, Xiaohang Zhan, Dahua Lin, Stella X. Yu, and Boqing Gong. Open Compound Domain Adaptation. In Proceedings of the IEEE/CVF Conference on Computer Vision and Pattern Recognition, 12:406-415, 2020.
- [9] Zhihe Lu, Yongxin Yang, Xiatian Zhu, Cong Liu, Yi-Zhe Song, and Tao Xiang. Stochastic Classifiers for Unsupervised Domain Adaptation. In Proceedings of the IEEE/CVF Conference on Computer Vision and Pattern Recognition, pages 9111–9120, 2020.
- [10] Bo Li, Yezhen Wang, Shanghang Zhang, Dongsheng Li, Trevor Darrell, Kurt Keutzer, and Han Zhao. Learning Invariant Representations and Risks for Semi-supervised Domain Adaptation. In Proceedings of the IEEE/CVF Conference on Computer Vision and Pattern Recognition, pages 1104–1113, 2021.
- [11] Ling Zhang, Xiaosong Wang, Dong Yang, Thomas Sanford, Stephanie Harmon, Baris Turkbey, Bradford J Wood, Holger Roth, Andriy Myronenko, Daguang Xu, et al. Generalizing Deep Learning for Medical Image Segmentation to Unseen Domains via Deep Stacked Transformation. *IEEE Transactions on Medical Imaging*, PP(99):1–1, 2020.
- [12] Riccardo Volpi, Hongseok Namkoong, Ozan Sener, John Duchi, Vittorio Murino, and Silvio Savarese. Generalizing to Unseen Domains via Adversarial Data Augmentation. In Advances in Neural Information Processing Systems (NIPS), 31:5334-5344, 2018.
- [13] Fengchun Qiao, Long Zhao, and Xi Peng. Learning to Learn Single Domain Generalization. In Proceedings of the IEEE/CVF Conference on Computer Vision and Pattern Recognition, pages 12556-12565, 2020.
- [14] Lei Li, Ke Gao, Juan Cao, Ziyao Huang, Yepeng Weng, Xiaoyue Mi, Zhengze Yu, Xiaoya Li, and Boyang xia. Progressive Domain Expansion Network for Single Domain Generalization. In Proceedings of the IEEE Conference on Computer Vision and Pattern Recognition (CVPR), 2021.
- [15] Hang Su, Subhransu Maji, Evangelos Kalogerakis, and Erik Learned-Miller. Multi-view Convolutional Neural Networks for 3D Shape Recognition. In IEEE International Conference on Computer Vision (ICCV), 2015.

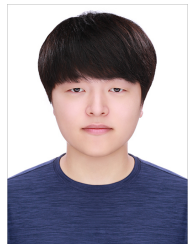
- [16] Yifan Feng, Zizhao Zhang, Xibin Zhao, Rongrong Ji, and Yue Gao. GVCNN: Group-View Convolutional Neural Networks for 3D Shape Recognition. In 2018 IEEE/CVF Conference on Computer Vision and Pattern Recognition, 2018.
- [17] Chu Wang, Marcello Pelillo, and Kaleem Siddiqi. Dominant Set Clustering and Pooling for Multi-View 3D Object Recognition. arXiv preprint arXiv:1906.01592, 2019.
- [18] Tan Yu, Jingjing Meng, and Junsong Yuan. Multi-view Harmonized Bilinear Network for 3D Object Recognition. In Proceedings of the IEEE Conference on Computer Vision and Pattern Recognition (CVPR), pages 186–194, 2018.
- [19] Abdullah Hamdi, Silvio Giancola, and Bernard Ghanem. MVTN: Multi-View Transformation Network for 3D Shape Recognition. In Proceedings of the IEEE/CVF International Conference on Computer Vision, pages 1–11, 2021.
- [20] Daniel Maturana, and Sebastian Scherer. VoxNet: A 3D Convolutional Neural Network for real-time object recognition. In 2015 IEEE/RSJ International Conference on Intelligent Robots and Systems (IROS), pages 922–928, 2015.
- [21] Zhirong Wu, Shuran Song, Aditya Khosla, Fisher Yu, Linguang Zhang, Xiaoou Tang, and Jianxiong Xiao. 3D ShapeNets: A Deep Representation for Volumetric Shapes. In Proceedings of the IEEE Conference on Computer Vision and Pattern Recognition (CVPR), pages 1912–1920, 2015.
- [22] Yangyan Li, Soeren Pirk, Hao Su, Charles R. Qi, and Leonidas J. Guibas. FPNN: Field Probing Neural Networks for 3D Data. In Advances in Neural Information Processing Systems (NIPS), 29, 2016.
- [23] Gernot Riegler, Ali Osman Ulusoy, and Andreas Geiger. OctNet: Learning Deep 3D Representations at High Resolutions. In Proceedings of the IEEE Conference on Computer Vision and Pattern Recognition (CVPR), pages 3577–3586, 2017.
- [24] Peng-Shuai Wang, Yang Liu, Yu-Xiao Guo, Chun-Yu Sun, and Xin Tong. O-CNN: Octree-based Convolutional Neural Networks for 3D Shape Analysis. ACM Transactions On Graphics (TOG), 36(4):1-11, 2017.
- [25] Andreas Geiger, Phillip Lenz, and Raquel Urtasun. Are we ready for autonomous driving? the kitti vision benchmark suite. In 2012 IEEE Conference on Computer Vision and Pattern Recognition, 2012.
- [26] Holger Caesar, Varun Bankiti, Alex H Lang, Sourabh Vora, Venice Erin Liong, Qiang Xu, Anush Krishnan, Yu Pan, Giancarlo Baldan, and Oscar Beijbom. nuScenes: A multimodal dataset for autonomous driving. In Proceedings of the IEEE/CVF conference on computer vision and pattern recognition, 2020.
- [27] MZhirong Wu, Shuran Song, Aditya Khosla, Fisher Yu, Linguang Zhang, Xiaoou Tang, and Jianxiong Xiao. 3D ShapeNets: A Deep Representation for Volumetric Shapes. In Proceedings of the IEEE Conference on Computer Vision and Pattern Recognition (CVPR), 2015.
- [28] Mikaela Angelina Uy, Quang-Hieu Pham, Binh-Son Hua, Duc Thanh Nguyen, and Sai Kit Yeung. Revisiting point cloud classification: A new benchmark dataset and classification model on real-world data. In International Conference on Computer Vision (ICCV), 2019.
- [29] Guocheng Qian, Yuchen Li, Houwen Peng, Jinjie Mai, Hasan Abed Al Kader Hammoud, Mohamed Elhoseiny, and Bernard Ghanem. PointNeXt: Revisiting PointNet++ with Improved Training and Scaling Strategies. arXiv preprint arXiv:2206.04670, 2022.
- [30] Lee, Rohee, Seonghoon Ryo, and Soomok Lee. "Domain-Invariant 3D Structural Convolutional Network for Autonomous Driving Point Cloud Dataset." 2024 IEEE Intelligent Vehicles Symposium (IV). IEEE, 2024.
- [31] Morai. Autonomous Vehicle Driving Simulator. Available online: <https://ko.morai.ai/> (accessed on 1 June 2023).
- [32] Soomok Lee, Sanghyun Lee, Jongmin Noh, et al. Special traffic event detection: framework, dataset generation, and deep neural network perspectives. Sensors (MDPI), 23(19):8129, 2023.
- [33] Soomok Lee and Seung-Woo Seo. Probabilistic context integration-based aircraft behaviour intention classification at airport ramps. IET Intelligent Transport Systems, 16(6):725–738, 2022.
- [34] Tero Karras, Samuli Laine, and Timo Aila. A Style-Based Generator Architecture for Generative Adversarial Networks. In Proceedings of the IEEE/CVF Conference on Computer Vision and Pattern Recognition, 2019.
- [35] Aaron van den Oord, Yazhe Li, and Oriol Vinyals. Representation Learning with Contrastive Predictive Coding. arXiv preprint arXiv:1807.03748, 2018.
- [36] Obata, Hiroto, and Chinthaka Premachandra. "Privacy-Secured Early Detection of Smartphone Users in Danger at Stations Using Depth Sensor and Deep Learning." 2024 IEEE International Symposium on Robotic and Sensors Environments (ROSE). IEEE, 2024.
- [37] Dingkan Liang, Xin Zhou, Wei Xu, Xingkui Zhu, Zhikang Zou, Xiaoqing Ye, Xiao Tan, and Xiang Bai. "PointMamba: A Simple State Space Model for Point Cloud Analysis." arXiv preprint arXiv:2402.10739v4, 2024.
- [38] Hengshuang Zhao, Li Jiang, Jiaya Jia, Philip Torr, and Vladlen Koltun. "Point Transformer," arXiv preprint arXiv:2012.09164v2, 2021.
- [39] Li Yi, Vladimir G Kim, Duygu Ceylan, I-Chao Shen, Mengyan Yan, Hao Su, Cewu Lu, Qixing Huang, Alla Sheffer, and Leonidas Guibas. "A scalable active framework for region annotation in 3d shape collections", ACM Transactions ON Graphics, 2016.
- [40] Zitong Yang, Yaodong Yu, Chong You, Jacob Steinhardt, and Yi Ma. "Rethinking Bias-Variance Trade-off for Generalization of Neural Networks", arXiv:2002.11328v3, 2020.
- [41] Yangyan Li, Rui Bu, Mingchao Sun, Wei Wu, Xinhan Di, Baoquan Chen. "PointCNN: Convolution On X-Transformed Points", Advances in neural information processing systems, vol. 31, pp. 820–830, 2018.
- [42] Jiaxin Li, Ben M Chen, and Gim Hee Lee. "SO-Net: SelfOrganizing Network for Point Cloud Analysis", In Proceedings of the IEEE Conference on Computer Vision and Pattern Recognition (CVPR), 2018.
- [43] Hugues Thomas, Charles R. Qi, Jean-Emmanuel Deschaud, Beatriz Marcotequi, Francois Goulette, and Leonidas J.Guibas. "KPConv: Flexible and Deformable Convolution for Point Clouds", In The IEEE International Conference on Computer Vision (ICCV), 2019.
- [44] Wenxuan Wu, Zhongang Qi, and Li Fuxin. "Pointconv: Deep convolutional networks on 3d point clouds", In Proceedings of the IEEE Conference on Computer Vision and Pattern Recognition (CVPR), 2019.
- [45] Yongcheng Liu, Bin Fan, Gaofeng Meng, Jiwen Lu, Shiming Xiang, and Chunhong Pan. "Densepoint: Learning densely contextual representation for efficient point cloud processing", In The IEEE International Conference on Computer Vision (ICCV), 2019.
- [46] Yongcheng Liu, Bin Fan, Shiming Xiang, and Chunhong Pan. "Relation-shape convolutional neural network for point cloud analysis", In Proceedings of the IEEE Conference on Computer Vision and Pattern Recognition (CVPR), 2019.
- [47] Xu Yan, Chaoda Zheng, Zhen Li, Sheng Wang, and Shuguang Cui. "Pointasnl: Robust point clouds processing using nonlocal neural networks with adaptive sampling", In Proceedings of the IEEE Conference on Computer Vision and Pattern Recognition (CVPR), 2020.
- [48] Yifan Xu, Tianqi Fan, Mingye Xu, Long Zeng, and Yu Qiao, "Spider-CNN: Deep Learning on Point Sets with Parameterized Convolutional Filters", In Proceedings of the European Conference on Computer Vision (ECCV), 2018.
- [49] Xiaoyang Wu, Yixing Lao, Li Jiang, Xihui Liu, Hengshuang Zhao, "Point Transformer V2: Grouped Vector Attention and Partition-based Pooling", In Advances in Neural Information Processing Systems (NIPS), 2022.
- [50] Changshuo Wang, Meiqing Wu, Siew-Kei Lam, Xin Ning, Shangshu Yu, Ruiping Wang, Weijun Li, Thambipillai Srikanthan, "GPSFormer: A Global Perception and Local Structure Fitting-based Transformer for Point Cloud Understanding", In Proceedings of the European Conference on Computer Vision (ECCV), 2024.
- [51] Faoxi Ran, Jun Liu, Chengjie Wang, "Surface Representation for Point Clouds", In Proceedings of the IEEE conference on computer vision and pattern recognition (CVPR), 2022.
- [52] Fei Yang, Franck Davoine, Huan Wang, and Zhong Jin, "Continuous Conditional Random Field Convolution for Point Cloud Segmentation", Pattern Recognition, Vol. 122, 2022.
- [53] Haotian Liu, Mu Cai, and Yong Jae Lee, "Masked Discrimination for Self-Supervised Learning on Point Clouds", In Proceedings of the European Conference on Computer Vision (ECCV), 2022.
- [54] Xumin Yu, Lulu Tang, Yongming Rao, Tiejun Huang, Jie Zhou, and Jiwen Lu, "Point-BERT: Pre-training 3D Point Cloud Transformers with Masked Point Modeling", , In Proceedings of the IEEE Conference on Computer Vision and Pattern Recognition (CVPR), 2022.
- [55] Hanchen Wang, Qi Liu, Xiangyu Yue, Joan Lasenby, and Matthew J. Kusner, "Unsupervised Point Cloud Pre-Training via Occlusion Completion", In The IEEE International Conference on Computer Vision (ICCV), 2021.
- [56] Yaohua Zha, Jinpeng Wang, Tao Dai, Bin Chen, Zhi Wang, and Shu-Tao Xia, "IDPT: Instance-aware Dynamic Prompt Tuning for Pre-trained Point Cloud Models", In The IEEE International Conference on Computer Vision (ICCV), 2023.
- [57] Meng-Hao Guo, Jun-Xiong Cai, Zheng-Ning Liu, Tai-Jiang Mu, Ralph R. Martin, and Shi-Min Hu, "PCT: Point cloud transformer", arXiv:2012.09688, 2020.
- [58] Mikaela Angelina Uy, Quang-Hieu Pham, Binh-Son Hua, Duc Thanh Nguyen, and Sai-Kit Yeung, "Revisiting Point Cloud Classification: A

New Benchmark Dataset and Classification Model on Real-World Data”, In The IEEE International Conference on Computer Vision (ICCV), 2019.

- [59] Hongyang Zhang, Yaodong Yu, Jiantao Jiao, Eric Xing, Laurent El Ghaoui, and Michael Jordan, ”Theoretically Principled Trade-off between Robustness and Accuracy”, Proceedings of the 36th International Conference on Machine Learning, PMLR 97:7472-7482, 2019.



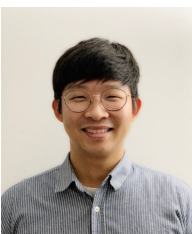
Younggun Kim received B.S. degree in mechanical engineering from Ajou University, Suwon, South Korea, in 2024. He is currently pursuing the M.S. degree in civil engineering with University of Central Florida, Florida, USA. His research interests include artificial intelligence, machine learning, and transportation.



Beomsik Cho received the B.S. degree in mechanical engineering from Ajou University, Suwon, South Korea, in 2023, where he is currently pursuing the M.S. degree in AI Mobility Engineering. His research interests include artificial intelligence, domain adaptation, and autonomous vehicles.



Seonghoon Ryo received the B.S. degree in mechanical engineering from Ajou University, Suwon, South Korea, in 2024, where he is currently pursuing the M.S. degree in AI Mobility Engineering. His research interests include artificial intelligence, object detection, and sensor fusion for autonomous vehicles.



Soomok Lee received the B.S. degree in Electrical Engineering from SungKyunKwan University, Seoul, Korea, in 2013 and the Ph.D. in Electrical and Computer Engineering from Seoul National University, Seoul, Korea, in 2019. Since 2022, he has been an Assistant Professor, with in the Department of Mobility Engineering and Department of Artificial Intelligence at AJOU University, Suwon, Korea. He is currently leading the Machine Learning & Mobility Laboratory as the Principal Investigator (PI). From 2013 to 2017, he was a researcher at SNU Intelligent Vehicle IT Center, Seoul, Korea. From 2017 to 2022, he was a Director of SW Engineering with ThorDrive, Inc, Ohio, USA. He performed 3D multi-modal deep learning-based fusion research as a Postdoctoral researcher at Harvard Medical School / Mass General Hospital at 2022. His current research areas include multi-modal sensor fusion, 3D computer vision, and domain adaptation.